Journal of Marine Science and Application (2026) 25: 1145-1159
https://doi.org/10.1007/s11804-026-00881-y

RESEARCH ARTICLE

Three-Dimensional Numerical Modeling of Wave-Induced Scour Around Caisson Breakwater Suspended on Piles

Rana N. Zedan[1], I. M. H. Rashwan[2], A. S. Koraim[3], Hany F. Abd-Elhamid[3,4], Martina Zeleňáková[5] and H. Omara[2]

Received: 24 March 2025 / Accepted: 02 August 2026
© Harbin Engineering University and Springer-Verlag GmbH Germany, part of Springer Nature 2026

Abstract

Scouring around vertical piles in ocean environments, especially under wave action, can significantly affect the stability of structures. Therefore, accurately predicting scour depth is essential for proper pile design. While empirical methods are commonly used, they often lack the accuracy required to model such complex processes, whereas data mining techniques provide more reliable predictions. This study evaluates the predictive performance of a morphological model for caisson breakwaters supported by piles under clear-water conditions, using the Flow-3D HYDRO mathematical modeling tool, addressing a gap in its application. In this study, a series of three-dimensional numerical models were developed to investigate the mechanisms of local scour around semi-immersed caisson breakwaters supported by piles. The investigation focused on key parameters such as the spacing between the piles and the gradual increase in the draft of the caisson barrier, subjected to different wave actions. The Reynolds-averaged Navier-Stokes (RANS) equations, along with the renormalization group (RNG) turbulence model and the Van Rijn sediment transport model, were used to simulate the morphological changes around the caisson breakwater. A numerical contour map was generated to assess the scour topography and sediment deposition beneath the breakwater and around the piles. A three-dimensional numerical model is developed to investigate modifying the caisson's cross section for different two scenarios on controlling the scour progress around a semi-immersed caisson suspended on piles under wave action. The simulation results were compared to previous experimental data, showing a high level of agreement. The effects of pile spacing on the flow field, bed elevation contours, deposition height, scour length, and scour depth were examined in two different scenarios with varying breakwater drafts. The findings reveal that pile spacing significantly affects the flow dynamics, local scour around the piles, and beneath the breakwater. This influence leads to distinctly different patterns of scour holes and variations in scour depth under the barrier. Detailed discussions are provided on the relationships between these effects and the dimensionless wave number. The attempt to increase the overall width of the breakwater by 0.25 W successfully moved scour away from the breakwater and the piles while maintaining its constant value

Keywords Breakwater; Caisson; Deposition; Piles; Scour

Article Highlights

- FLOW-3D HYDRO accurately reproduced the hydrodynamic and seabed responses of pile-supported caisson breakwaters.
- Maximum scour occurred at Kh = 0.7–0.9, with relative scour depths of 0.10–0.12.
- Increasing the breakwater width by 0.25 W effectively redirected scour away from the piles without increasing scour depth.

✉ Hany F. Abd-Elhamid
hany.abdelhamid@tuke.sk

[1] Civil Engineering Department, Faculty of Engineering, Delta University for Science and Technology, Gamasa 11152, Egypt

[2] Irrigation and Hydraulics Engineering Department, Faculty of Engineering, Tanta University, Tanta 31527, Egypt

[3] Department of Water and Water Structures Engineering, Faculty of Engineering, Zagazig University, Zagazig 44519, Egypt

[4] Department of Environmental Engineering, Faculty of Civil Engineering, Technical University of Kosice, 040 01 Košice, Slovakia

[5] Institute of Sustainable and Circular Construction, Faculty of Civil Engineering, Technical University of Kosice, 040 01 Košice, Slovakia

1 Introduction

Groups of piles are typically accustomed to sustenance maritime constructions, with their procedure carefully selected to ensure strong structural integrity against wave forces. However, the piles arrangement also affects wave hydrodynamics, leading to changes such as flow contraction and the formation of stormy vortices everywhere in the piles. This results in increased bed shear stress, leading to scour that can significantly threaten the structural stability of the piles. The risk is especially elevated during storm conditions, when wave flow characteristics shift dramatically, causing rapid scouring. Consequently, a thorough analysis of wave-induced scour around a group of piles is essential.

In many coastal areas, breakwaters are traditional structures constructed along the shore to prevent erosion from strong waves. As noted by Vitousek et al. (2017), breakwaters will likely need to adapt to various climate change impacts, including rising sea levels, more forceful waves,

alterations in the cradle outline, and intensified storms. These alterations result in heightened wave effects on coastal barriers. The interaction of waves with the barrier causes significant barrier scour, which is considered a major factor in seawall failure, particularly because vertical seawalls are ineffective at dissipating wave energy (Kraus and McDougal, 1996). Consequently, although seawalls are effective in safeguarding against coastal erosion, it is essential to evaluate the scour around breakwaters to maintain their structural integrity.

The breakwater scour occurs when a wave strikes the barrier, causing water to rush up the structure and form a vertical jet at the still water level. This consequences in increasing scour at the breakwater's toenail. Additionally, as the water is replicated back seaward after impact, the area near the seawall becomes more prone to scour. Seawall scour has been examined in prior studies through a combination of observational and laboratory research. Dean (1987) evaluated the impact of seawalls on the shoreline, discovering that their presence results in a steeper seabed profile and heightened scour at the base of the seawall.

Kamphuis et al. (1992) carried out a three-dimensional experimental study on seawall scour and longshore sediment transport. They found that as the scour depth at the seawall increases, the rate of longshore sedimentation in front of the barrier decreases. In a significant two-dimensional scour experiment, Sumer and Fredsoe (2000) studied a vertical breakwater located on a smooth seabed and exposed to both regular and irregular waves. Their results indicated that the patterns of scour and deposition alternated between the two processes. Additionally, they found that irregular waves resulted in shallower scour depths compared to regular waves. Sutherland et al. (2006) examined how inclined and vertical seawalls affect seabed scour and found that the maximum scour depth is prejudiced by the surf similarity parameter and the relative water depth at the seawall's toe. Their study also indicated that the seawall's slope does not impact the maximum scour depth; inclined seawalls produced scour depths similar to those of vertical seawalls. Tsai et al. (2009) investigated seawall scour caused by breaking waves and discovered that an increase in water level at the base of the seawall leads to a decrease in maximum scour depth. Heikal et al. (2022) conducted experimental research on the effectiveness of caisson breakwaters supported by piles, examining their impact on erosion and sedimentation processes in nearby coastal areas. Progress in mathematical modeling of cross-shore sediment transport under breaking waves has been limited. Roelvink and Stive (1989) explored the mechanisms affecting cross-shore flow and seabed profile changes caused by random waves, suggesting that these changes result from return flow and increased bed shear forces due to wave breaking on sloped beds.

McDougal et al. (1997) were pioneers in developing a numerical model of the cross-shore profile involving a seawall. Their analysis utilized a simple computational framework based on empirical formulas for sediment and wave dynamics, examining how reflected waves impacted sediment movement along the shore and revealing that reflected waves from the seawall significantly influence nearby seabed profiling. Gíslason et al. (2009) used a sediment transport model to address the Reynolds-Averaged Navier-Stokes (RANS) equations, investigating standing wave formation and the subsequent scour at a breakwater on a flat-bed. Their findings, consistent with those of Sumer and Fredsoe (2000), indicated that the ratio of scour depth (S) to wave height (H_o) decreases with increasing water depth, although their estimates did not consider the effects of a sloped seabed and wave breaking. To model non-breaking waves, they employed a kinematic boundary condition based on free surface volume flow. Myrhaug and Ong (2009) introduced a stochastic method to estimate random wave-induced scour depth at the trunk section of vertical wall and rubble-mound breakwaters. By treating the waves as a stationary Gaussian narrow-band random process, they applied formulas for scour depth induced by regular waves, as outlined by Sumer and Fredsoe (2000) and Xie (1981), to calculate the scour depth for random waves. Baykal et al. (2015) found that excluding the suspended load resulted in a 50% reduction in the calculated scour depth around a vertical pile in a steady current.

Baykal et al. (2015) found that neglecting the suspended load led to a 50% reduction in calculated scour depth around a vertical pile under a steady current. Baykal et al. (2017) investigated the effect of wave conditions on equilibrium scour depth and found encouraging results for backfilling the scour hole under wave action. Ahmad et al. (2019) studied the mathematical modeling of an arctic bluff with a sloping bed, simulating the scouring process using RANS equations and a sediment transport model. They used the level-set method (LSM) to capture the free surface, including breaking waves. The study illustrated how wave breaking and scour develop along a vertical bluff through hydrodynamic analysis.

Yang et al. (2024) investigated local scour around an artificial reef in steady currents, finding that increased opening numbers led to reductions in both scour volume and depth. Currently, physical modeling remains the most effective method for evaluating local scour around complex breakwater shapes that exceed the assumptions of existing scour equations. Although three-dimensional (3D) numerical modeling (FLOW-3D HYDRO) has been successful in simulating local scour around a single cylindrical pile, there remains a significant gap in numerical studies of scour under caisson breakwaters, particularly those focusing on groups of piles as foundations subjected to wave action. This study aims to assess; (1) The skill of the model to forecast the scour mechanism around the semi-

immersed caisson breakwater suspended on a group of piles, and (2) The scour (scour depth and hole contours) around semi-immersed caisson breakwater suspended on a piles system under various environmental conditions.

2 Description of the FLOW-3D model

Underwater flow conditions can be modeled using the FLOW-3D HYDRO model to assess seabed and suspended load rates. This model solves the 3D Navier-Stokes equations with a non-hydrostatic finite variation approach, making it effective for simulating free surface flow and sediment transport, including deposition and entrainment. The FLOW-3D HYDRO model predicts sediment migration and degradation through empirical equations, a nonlinear drift flux method, and a bed load transfer model. Additionally, it employs a volume tracking algorithm and vortex analysis in box tests. The FAVOR approach is used to delineate domain boundaries and identify areas of flow obstruction (Lin et al., 2014).

2.1 Hydrodynamic model

In this study, the RANS equations were numerically solved using the simpler renormalization group (RNG) turbulence model to enhance computational efficiency. The RNG model was chosen for the following reasons: (1) It performs well in simulating turbulent flow in general and is more broadly applicable than the conventional (k-ε) model for scenarios involving breakwater piles, (2) It is considered one of the most robust and accurate models for scour simulations, and (3) the RNG model is particularly effective for scour predictions in situations where the fluid generates a high degree of turbulence as it flows through breakwater structures.

2.1.1 Reflection, and transmission coefficient

The reflection (K_r) and the transmission (K_t) coefficients can be expected as:

$$K_r = \frac{H_r}{H_i} \tag{1}$$

$$K_t = \frac{H_t}{H_i} \tag{2}$$

where K_r is the reflection coefficient, and K_t is the transmission coefficient, H_i is the incident wave height, H_t is the transmitted wave height, and H_r is the reflected wave height.

2.2 Sediment scours model

This model assumes the presence of non-cohesive sediment and estimates sediment transport by predicting the processes of erosion, advection, and deposition. The Soulsby-Whitehouse equation (Wei et al., 2014) is utilized to estimate the critical Shields parameter. The dimensionless parameter, T, is calculated as follows:

$$T = d\left(\frac{\rho\left(\rho_s - \rho\right)g}{\mu^2}\right)^{1/3} \tag{3}$$

where μ represents the dynamic viscosity of the fluid, ρ_s denotes the sediment density, ρ indicates the fluid density, d is the particle diameter, and g is the acceleration due to gravity. The Soulsby-Whitehouse equation is used to compute the dimensionless critical shields parameter θ_{cr} in the form of formulas:

$$\theta_{\mathrm{cr}} = \frac{0.3}{1 + 0.2T} + 0.055\left(1 - \exp\left(-0.02T\right)\right) \tag{4}$$

The local shields parameter θ_i in (5) is calculated using the local bed shear stress τ:

$$\theta_i = \frac{\tau}{\left\| g \right\| d_i\left(\rho_i - \rho_f\right)} \tag{5}$$

The entrainment coefficient can be employed to scale scour rates or calibrate experimental data with a value of 0.005 yielding satisfactory results. The volumetric sediment transport rate per width of bed Van Rijn Equation (6) which has been defined as follows is used,

$$\varphi_i = \beta_{\mathrm{VR},\, i^{d_*^{-0.3}},\, i}\left[\frac{\theta}{\theta'_{\mathrm{cr},\, i}} - 1\right]^{2.1} c_{b,\, i} \tag{6}$$

where $\beta_{\mathrm{VR},\, i^{d_*^{-0.3}},\, i}$ is a coefficient that is naturally equal to 0.053, $c_{b,\, i}$ is the volume fraction of species i in the bed material, and ϕ_i is the dimensionless cradle consignment conveyance degree, which is assumed to be 0.05.

3 Computational domain

The FLOW-3D HYDRO model was validated using experimental data from Koraim (2005). Before the simulation, a numerical wave flume and the geometry of a semi-immersed caisson breakwater supported by a pile system on sandy soil were created using FLOW-3D HYDRO. Figure 1 illustrates the breakwater models and the cradle geography data. The cradle geography around and beneath the breakwater models were recorded to assess equilibrium erosion and accretion, with the mean water depth maintained at 20 cm. The dimensions and conditions of the tested models are detailed in Table 1 by Koraim (2005).

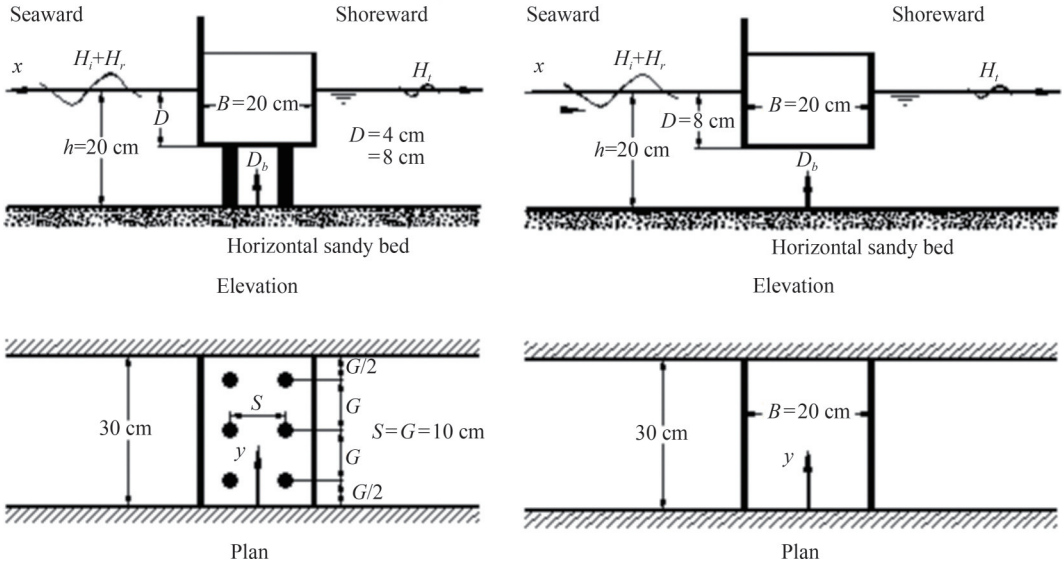


Figure 1 The details of the models on a sandy be (Koraim, 2005)

Table 1 The details of the models were tested on a sand bed

Parameter	Values
Breakwater width (B) (cm)	20
Breakwater draft (D) (cm)	4 and 8
Pile diameter (d) (cm)	3.3
Water depth (h) (cm)	20
Relative pile diameter (d/h)	0.165
Pile gapping (G) (cm)	10
Relative pile gapping (G/h)	0.5
Pile spacing (S) (cm)	10
Bed slope (s_b)	0%
Wave periods (T) (s)	1.0, 1.2, 1.5, 2.0, and 3.0
Dimensionless wave number (Kh)	1.32, 1.00, 0.80, 0.62, 0.46, and 0.26
Wave height (H_i) (m)	0.085, 0.088, 0.073, 0.049, and 0.045

Before validating the model, it needed to be dimensionally calibrated. The morphological domain dimensions were set to match those of the experimental flume used by Koraim (2005), with a width of 30 cm and a height of 45 cm. Considerable effort was invested in ensuring that the domain length was adequate to accurately capture the scour behavior observed in the experiments.

A sufficient gap was needed between the pile system and the wave absorber to ensure proper wave reflection. This gap should be 80 times the pile diameter (d), while the distance between the wave inlet and the pile system should be 32 times the pile diameter (d), as shown in Figure 2. To allow the wave to fully develop and to prevent initial scour, a fixed bed was established at the inlet of the domain.

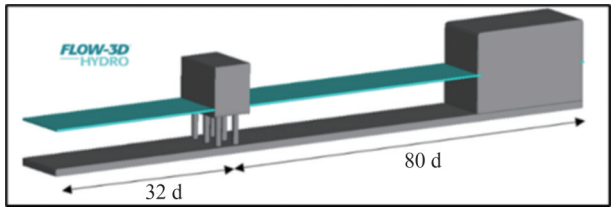


Figure 2 Numerical model length

In FLOW-3D, the grid spacing plays a vital role in the simulation process. The mesh resolution directly affects the computational time, with finer grids generally increasing the runtime. To accurately simulate the development of scour, smaller mesh elements were applied around the piles and along the beach bed. In particular, cell sizes of 30, 25, 20, 15, 10, 5, and 1 mm were tested in these areas to determine the most suitable resolution for the study. The optimal cell size was identified by assessing when the simulated scour depth became stable and showed no significant variations, as illustrated in Figure 3.

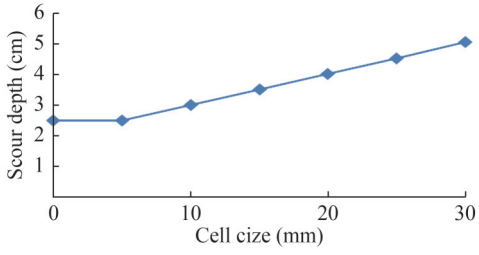


Figure 3 Effect of cell size on scour depth

Figure 3 indicates that the scour depth stabilizes and becomes independent of the grid resolution when the cell size is smaller than 5 mm. However, using a coarser grid, such as a 30 mm cell size, led to noticeable inaccuracies.

Consequently, a 5 mm cell size was selected as the optimal resolution to achieve accurate results and a reliable representation of the scour depth around the piles. The computational domain was divided into three mesh blocks of different sizes and boundary conditions to simulate the experimental flume. Among these, Mesh Block 2 contained the pile model and was assigned the finest grid to enhance the accuracy of the simulation outcomes.

To better capture the scour development around the piles, two mesh regions with higher refinement were generated on both sides of the piles along the x and y directions. The smallest cell size near the piles was set to 5 mm and gradually expanded to 20 mm away from them to optimize computational efficiency. These mesh parameters were determined through a trial-and-error approach to ensure good agreement between the simulation and experimental results. The final mesh consisted of 316 700 cells assigned to the workstation, as illustrated in Figure 4.

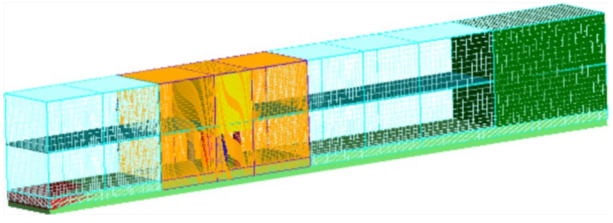


Figure 4 The meshing plane structure around the piles

One of the main challenges in the numerical modeling process lies in selecting suitable scour parameters to achieve results that closely align with experimental observations. Extensive effort was dedicated to this task, as parameters such as the critical Shields parameter, entrainment coefficient, and bed load coefficient play a crucial role in model accuracy. Through multiple trial-and-error simulations, the optimal parameter values were identified as follows: critical Shields parameter = 0.045, entrainment coefficient = 0.005, and bed load coefficient = 0.053. Among these, the entrainment coefficient proved to be the most influential, as even minor adjustments to its value led to significant variations in the predicted erosion results.

Table 2 displays the mechanical properties of the sediment, based on the experimental work of Koraim (2005) and utilized in this numerical study. The values presented in the table were determined during the model calibration process.

Determining the appropriate boundary circumstances for the hydraulic investigation is a crucial step in the numerical imitation. After applying these boundary circumstances to the numerical model and calibrating several key parameters that directly influence the results, the simulation's accuracy was verified by comparing the numerical outcomes with experimental data. The boundary circumstances for the computational field are outlined in Figure 5. The FLOW-3D model defined the top surface for each run, corresponding to stagnation pressure and atmospheric pressure (P) across the three blocks. A sediment layer 0.15 meters thick was placed at the bottommost of the model with a wall boundary condition (W) applied there. Additionally, wall boundaries (W) were set on the right and left sides of the numerical domain.

Table 2 Mechanical properties of the sediment

Diameter	Density (kg/m^3)	Entrainment coefficient	Bed load coefficient	The angle of repose (°)	Maximum packing fraction
0.0002	2050	0.005	0.053	32	0.52

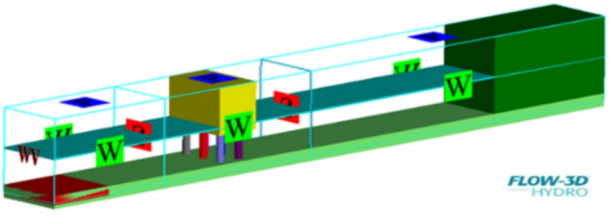


Figure 5 Boundary conditions of the numerical model

For block 1, the inlet boundary condition was set to a 5th-order Stokes wave (WV), while the outlet was assigned a symmetry boundary condition (S). To improve computational efficiency, the inlet and outlet boundary conditions for block 2 were also set as symmetry boundary conditions (S). In block 3, the inlet boundary condition was set to symmetry (S), and the outlet boundary condition was configured as a wall condition (W) with an absorbing wave block. The boundary circumstances of the numerical model were designed to match the physical conditions of the problem. Once these requirements are met, the model is ready for use in various scenarios. Calculations requiring 10 minutes of physical time typically need about one day's worth of workstation processing (using 14 processors).

4 Results and discussion

4.1 Verification of hydrodynamic model

Figure 6 presents a comparison of the transmission coefficient K_t values between Koraim (2005) experimental results and the present FLOW-3D HYDRO results when the dimensionless wave number Kh = 0.8. Five ethics of breakwater drafting D (D = 0, 0.04, 0.08, 0.12, and 0.16 m) were applied. The percentage errors for different values of changing the relative breakwater gaping G/h are 9.52% for G/h = 0.50, 7.60% for G/h = 0.75, and 12.50% for G/h = 1.50, Table 3.

Figure 7 presents a comparison of the transmission coefficient K_r values between Koraim (2005) experimental

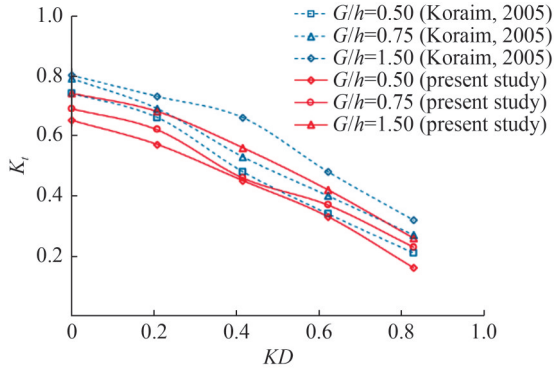


Figure 6 The CFD results versus Koraim (2005) the experimental results of the effect of *KD* on K_t at different *G*/*h* values

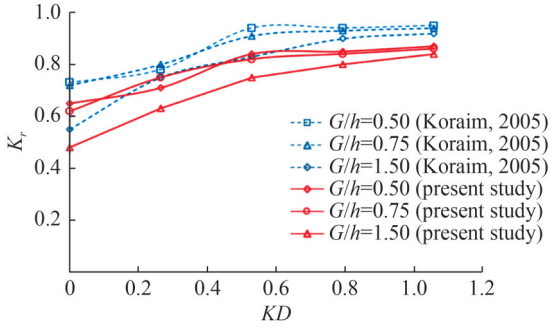


Figure 7 The CFD results versus Koraim (2005) the experimental results of the effect of *KD* on K_r at different *G*/*h* values

results and the present FLOW-3D HYDRO results when the dimensionless wave number *Kh* = 0.8. Five ethics of breakwater drafting *D* (*D* = 0, 0.04, 0.08, 0.12, and 0.16 m) were applied. The percentage errors for different values of changing the relative breakwater gaping *G*/*h* are 9.47% for *G*/*h* = 0.50, 7.60% for *G*/*h* = 0.75, and 8.57% for *G*/*h* = 1.50, Table 4.

4.2 Verification of morphological model

4.2.1 Seabed changes for Kh = 0.8

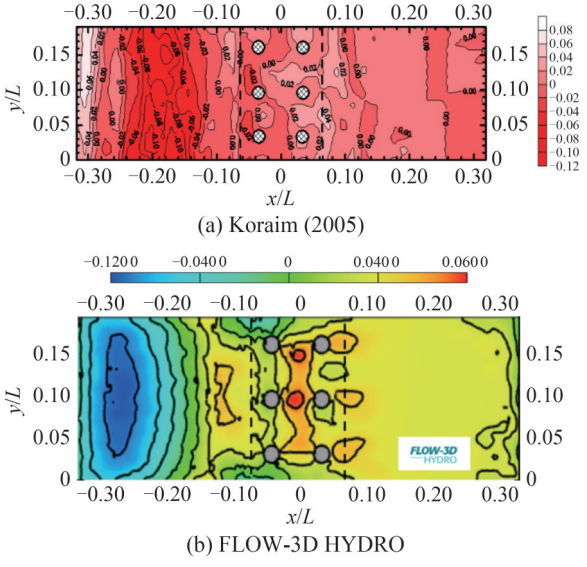
Figures 8 and 9 present a comparison contour maps between the Koraim (2005) experimental results and the present FLOW-3D HYDRO model for the seabed changes under and around the pile system supported the caisson breakwater when the dimensionless wave number *Kh* = 0.80, For two cases of changing the relative breakwater drafting *D*/*h* =0.20 (closely spaced piles), and *D*/*h*= 0.40 (large spaced piles). The Figures indicated that the maximum sea bed scours were induced at a distance away from the seaward tip breakwater. Also, there are random small deposition zones appear in a different location along the contour maps. From Figure 8, the observed seaward D_{smax}/h is 0.120 for the experimental and numerical contour map as the D_{smax} seaward represents 12% relative to the water depth. Also, D_{smax}/h around the supporting piles is 0.030 from the experimental model and 0.020 from the numerical model with Dsmax equal to 3% and 2% relative to the water depth for the experimental and numerical results respectively. The maximum shoreward deposition height D_{dmax}/h is 0.050 from the experimental model and 0.060 from the numerical model. The experimental scour hole length L_{smax}/l seaward and everywhere the piles are 0.160 and 0.060 while 0.140 and 0.040 from the numerical model.

Table 3 Percentage relative error on K_t values

KD	*G*/*h* = 0.5			*G*/*h* = 0.75			*G*/*h* = 1.50		
	Exp.	Num.	Relative error (%)	Exp.	Num.	Relative error (%)	Exp.	Num.	Relative error (%)
0.00	0.70	0.67	4.29	0.77	0.73	5.19	0.84	0.79	5.59
0.21	0.59	0.54	8.48	0.68	0.62	8.82	0.71	0.65	8.45
0.41	0.45	0.42	6.67	0.52	0.49	5.77	0.54	0.5	7.41
0.62	0.30	0.29	1.67	0.36	0.33	8.33	0.46	0.43	6.52
0.83	0.18	0.17	5.56	0.24	0.235	2.08	0.28	0.26	7.14

Table 4 Percentage relative error on K_r values

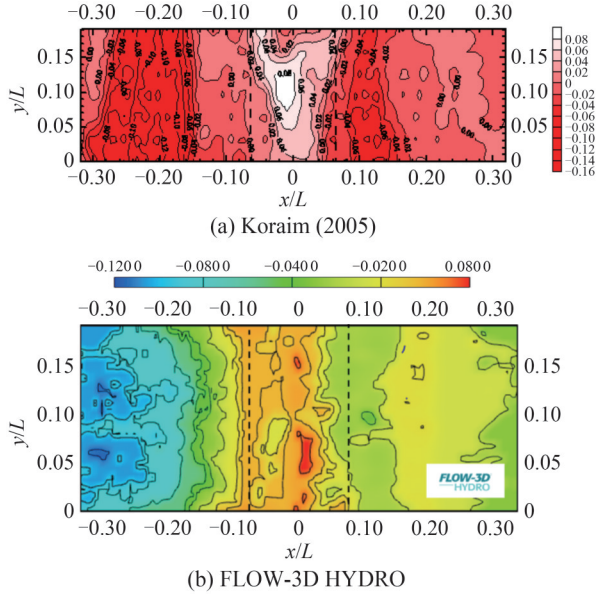
KD	*G*/*h* = 0.5			*G*/*h* = 0.75			*G*/*h* = 1.50		
	Exp.	Num.	Relative error (%)	Exp.	Num.	Relative error (%)	Exp.	Num.	Relative error (%)
0.00	0.68	0.64	5.88	0.49	0.74	4.08	0.52	0.49	5.77
0.21	0.72	0.68	5.56	0.61	0.59	3.28	0.55	0.52	5.45
0.41	0.88	0.82	6.82	0.80	0.74	7.50	0.70	0.64	8.57
0.62	0.95	0.86	9.47	0.88	0.83	5.68	0.75	0.69	8.00
0.83	0.96	0.88	8.33	0.92	0.85	7.60	0.81	0.78	3.70



(a) Koraim (2005)

(b) FLOW-3D HYDRO

Figure 8 Comparison between two contour maps for the case of $Kh = 0.80$ and $D/h = 0.20$ (closely spaced piles)



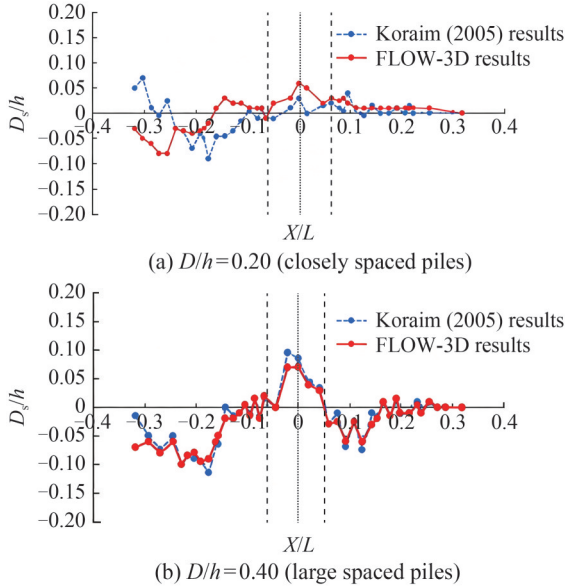
(a) Koraim (2005)

(b) FLOW-3D HYDRO

Figure 9 Comparison between two contour maps for the case of $Kh = 0.80$ and $D/h = 0.40$ (large spaced piles)

Figure 9 indicated that the experimental and numerical contour maps confirmed that there are two scour holes, the biggest one formed seaward with D_{smax}/h and L_{smax}/l are 0.120 and 0.160 for the experimental contour maps while 0.120 and 0.180 for the numerical contour maps. While the smallest formed shoreward with D_{smax}/h and L_{smax}/l are 0.060 and 0.120 for the experimental contour map and 0.050 and 0.120 for the numerical contour map. Also, the maximum shoreward deposition height is 0.030 for the experimental contour map and 0.050 for the numerical contour map. That means that the FLOW-3D model succeeds in predicting the sea bed scour and deposition for the intermediate wave with different cases of changing the relative breakwater drafting.

Figures 10(a) and 10(b) compare the longitudinal seabed profiles at the center of the flume domain, showing both the experimental results from Koraim (2005) and the current FLOW-3D numerical results for $Kh = 0.80$. The comparisons are made for different configurations: $D/h = 0.20$ (closely spaced piles), and $D/h = 0.40$ (widely spaced piles). The figures reveal a high degree of conventual between the experimental and mathematical outcomes in the patterns of erosion and deposition.



(a) D/h=0.20 (closely spaced piles)

(b) D/h=0.40 (large spaced piles)

Figure 10 Comparison between the experimental and numerical longitudinal cross-section of the seabed profile when $Kh = 0.80$ for different breakwater drafting

4.2.2 Seabed changes for Kh = 0.26

Figures 11, 12 and 13 present an assessment contour maps between the Koraim (2005) experimental results and the present FLOW-3D HYDRO model for the seabed changes under and around the pile system supported the caisson breakwater when the dimensionless wave number $Kh = 0.26$, For three cases of changing the relative breakwater drafting $D/h = 0.20$ (closely spaced piles), and $D/h = 0.40$ (closely spaced piles), and $D/h = 0.40$ (large spaced piles).

For Figure 11 and Figure 12, different scour zones formed around the pile system and there is deposition zones formed near shoreward for both numerical and experimental contour maps. Figure 11 indicated that D_{smax}/h, and L_{smax}/l seaward are 0.050 and 0.010 for the experimental contour map but 0.040 and 0.010 for the numerical contour map. While D_{dmax}/h is 0.040 for the experimental contour map and 0.035 for the numerical contour map. Figure 12 indicated that D_{smax}/h seaward is 0.090 for the experimental contour map and 0.080 for the numerical contour map.

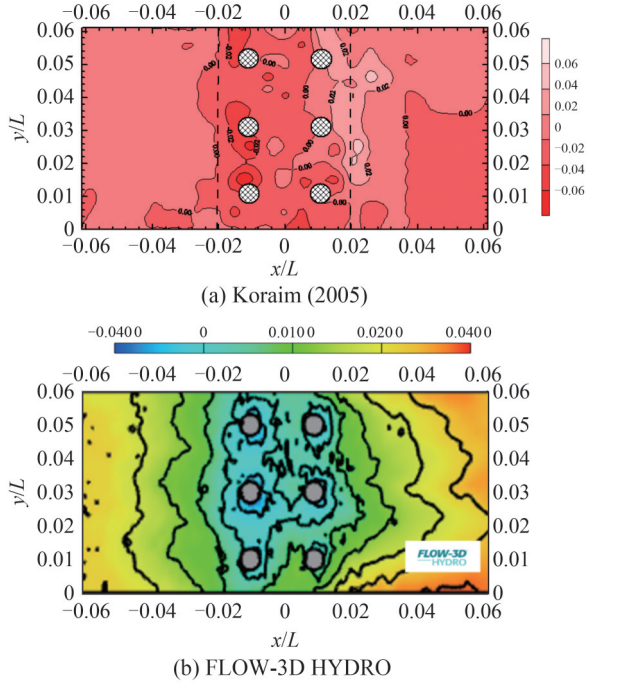


Figure 11 Comparison between two contour maps for the case of Kh = 0.26 and D/h = 0.20 (closely spaced piles)

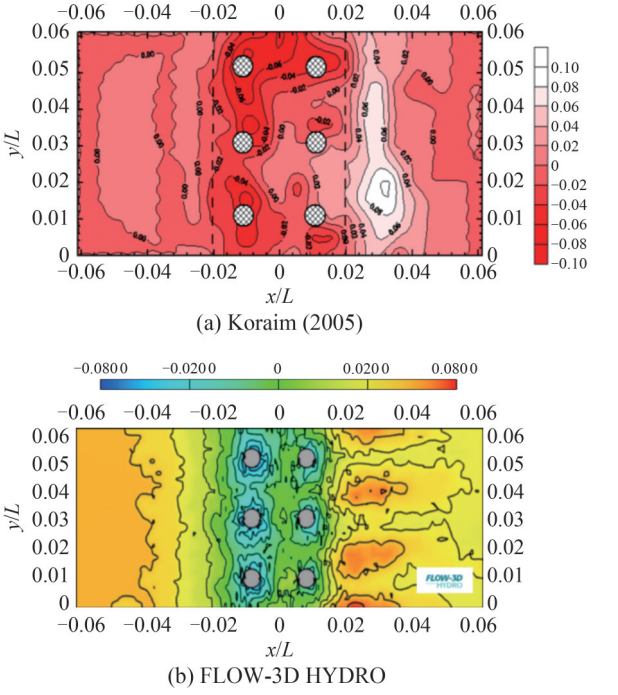


Figure 12 Comparison between two contour maps for the case of Kh = 0.26 and D/h = 0.40 (closely spaced piles)

D_{dmax}/h is 0.090 for the experimental contour map and 0.080 for the numerical contour map. Also, L_{smax}/l is 0.040 for the experimental contour map and 0.050 for the numerical contour map. Figure 13 indicates that the effect of increasing D/h to 0.40 in the case of large-spaced piles

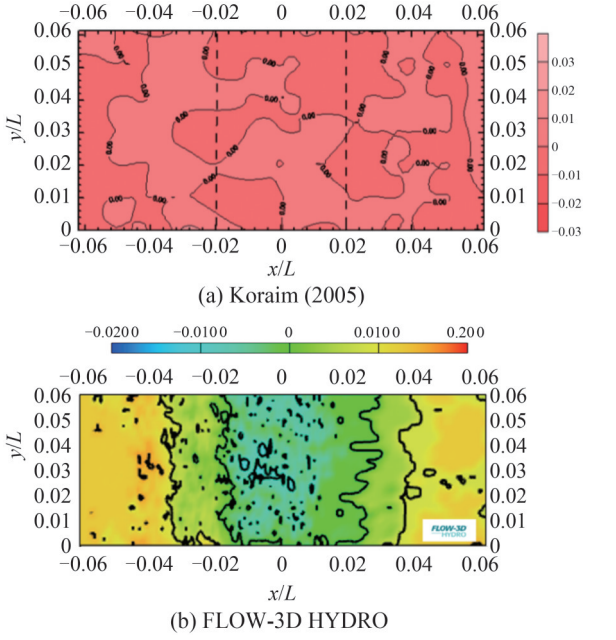


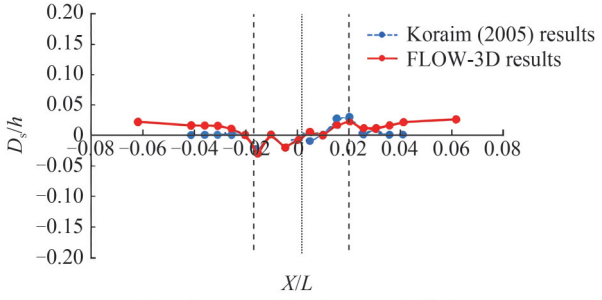
Figure 13 Comparison between two contour maps for the case of Kh = 0.26 and D/h = 0.40 (large spaced piles)

on the sea bed profile is very minor and can be ignored. Figure 14 presented a comparison between the numerical and experimental longitudinal cross-section of the sea bed pattern at the middle of the wave flume when Kh = 0.26 for different D/h values. The figure proved that the seabed profile is not regular because of the high confusion caused by the interaction between the incident and the reflected waves beside the wave breaking and the horseshoe vortex formed in front of the breakwater system for both numerical and experimental profiles. Figure 14 presented a high matching between the sea bed profile for the experimental and numerical results.

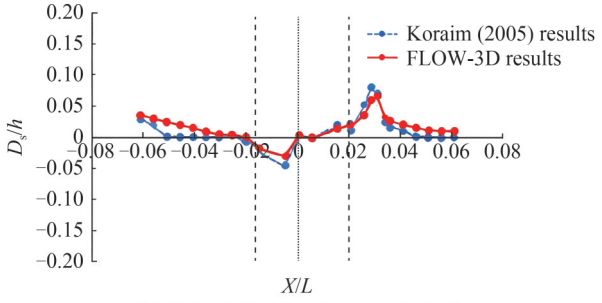
The following Table 5 depicts the mean square error (M. S. E) values between the experimental and the numerical results for the longitudinal seabed changes at the middle of the contour maps for different cases of changing Kh under various scenarios of D/h. The results are based on the following (Eq. 7):

$$\mathrm{MSE} = \frac{1}{n_s}\sum_{n=1}^{n=n}\left(Y_{\mathrm{exp}} - Y_n\right)^2 \tag{7}$$

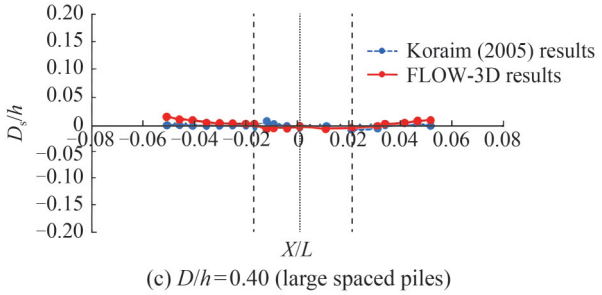
where n_s is the number of samples, Y_{exp} is the experimental values, and Y_n is the numerical values. Table 5 indicated that in the case of Kh = 0.80 for D/h = 0.40 (closely spaced piles) the M.S.E recorded a high error with 0.002 092 compared with the other values. The best M.S.E value is 0.000 031 for the case of Kh = 1.32 when D/h = 0.40 (large spaced piles). That means that the validation of the medium wave for example Kh = 0.80 with FLOW-3D HYDRO recorded low convergence between the numerical results and the experimental results, especially in the case of existence piles.



(a) D/h=0.20 (closely spaced piles)



(b) D/h=0.40 (closely spaced piles)



(c) D/h=0.40 (large spaced piles)

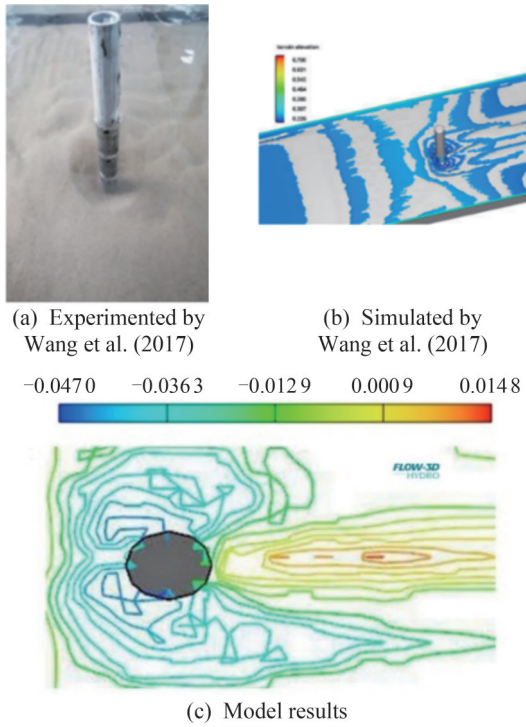
Figure 14 Comparison between the experimental and numerical longitudinal cross-section of the seabed profile when Kh = 0.26 for different breakwater drafting

Table 5 Mean square error for different validated data

Kh	D/h	MSE
1.32	D/h = 0.2 (closely spaced piles)	0.000 243 3
	D/h = 0.4 (large spaced piles)	0.000 031
0.80	D/h = 0.2 (closely spaced piles)	0.001 765
	D/h = 0.4 (closely spaced piles)	0.002 092
	D/h = 0.4 (large spaced piles)	0.000 161
0.26	D/h = 0.2 (closely spaced piles)	0.000 17
	D/h = 0.4 (closely spaced piles)	0.000 135
	D/h = 0.4 (large spaced piles)	0.000 057 894 7

While the results of large-spaced piles recorded high convergence between the numerical results and the experimental results.

Figures 15(a) and 15(b) show a comparison of the results of the bed topography at (t = 20 min) observed experimentally and numerically by Wang et al. (2017) and simulated numerically in this research by FLOW-3D HYDRO. Figure 15(c) presents the simulated scour contour map by FLOW-3D HYDRO. It is noticed that the maximum scour depth is 0.045 0, and 0.047 0 for the experimental and numerical results of Wang et al. (2017), respectively. The maximum scour depth received by the present model is 0.046 5. For that, the present FLOW-3D HYDRO model gives the perfect agreement with the experimental and numerical (Wang et al., 2017) with a mean square error equal to 0.000 012 5. Therefore, the FLOW-3D HYDRO simulates the bed changes around piles with high accuracy.



(a) Experimented by Wang et al. (2017)

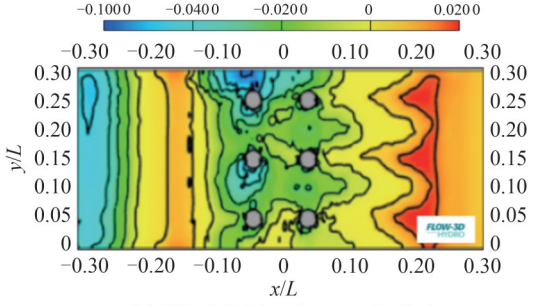
(b) Simulated by Wang et al. (2017)

(c) Model results

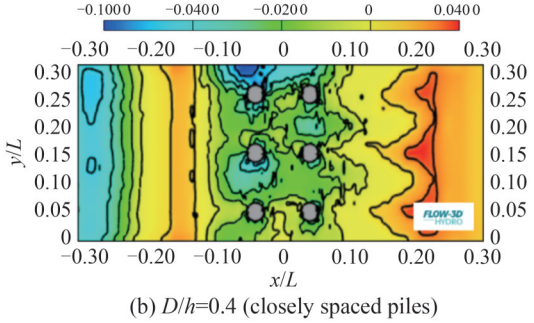
Figure 15 Scour hole contours at (t = 20 min)

4.2.3 Seabed changes for Kh = 1

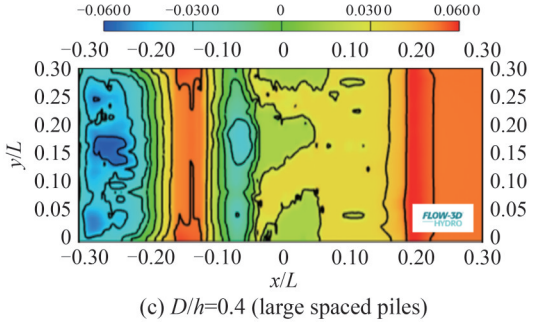
Figure 16 presents the numerical sea bed morphology of the three breakwater models when Kh = 1 for three cases of changing the relative breakwater drafting D/h. The first model for D/h = 0.2 (closely spaced piles), the second model for D/h = 0.4 (closely spaced piles), and the third model for D/h = 0.4 (large spaced piles). The figure presented that for the three breakwater models, two scour holes were formed, the first scour hole was formed seaward while the second scour hole was formed around the piles under the breakwater system with a big erosion under one



(a) D/h=0.2 (closely spaced piles)



(b) D/h=0.4 (closely spaced piles)



(c) D/h=0.4 (large spaced piles)

Figure16 Contour maps of the seabed changes around the different caisson breakwater models when $Kh = 1$

side pile. Also, one big deposition height formed shoreward. For the first model given in Figure 16(a) the maximum relative seaward scour depth D_{smax}/h is 0.08. The D_{smax}/h around-the-side pile is 0.09 and under the breakwater system is 0.03. The maximum shoreward relative deposition height D_{dmax}/h is 0.02. The relative scour hole lengths L_{smax}/l seaward and around the piles are 0.18 and 0.10. For the second model given in Figure 16(b) the maximum relative seaward scour depth D_{smax}/h is 0.08. The D_{smax}/h around the side pile is 0.10 and under the breakwater system is 0.03. The maximum shoreward relative deposition height D_{dmax}/h is 0.04. The extreme relative scour hole lengths L_{smax}/l seaward and around the piles are 0.18 and 0.10. As shown in the first and the second models, there is little difference observed in changing sea bed morphology when increasing the relative breakwater drafting for $Kh = 1$. For the third model presented in Figure 16(c), different scour and deposition zones appear along the contour map. The extreme relative seaward scour depth D_{smax}/h is 0.06. The extreme relative scour depth under the breakwater system D_{smax}/h is 0.02. The maximum relative deposition height D_{smax}/h is 0.06. The extreme relative scour hole length L_{smax}/l is 0.16.

Figure 17 presented the numerical longitudinal sea bed pattern at the center of the contour map for the three breakwater models when $Kh = 1$ for different ethics of changing the relative breakwater drafting D/h. The figure shows that the sea bed morphology is not uniform but varies from scour zones to deposition zones. Also, increasing D/h from 0.2 to 0.4 in the case of closely spaced piles doesn't give more changes in the seabed profile. As there are little scour holes around the piles and big deposition height shoreward. But in the case of $D/h = 0.4$ (Large spaced piles), the scour decreased under the breakwater system and concentrated under the tip of the breakwater with a big deposition height shoreward. The distribution of the scour and deposition zones exerted from FLOW-3D Hydro when $Kh = 1$ for the three breakwater models is presented in Figure 18.

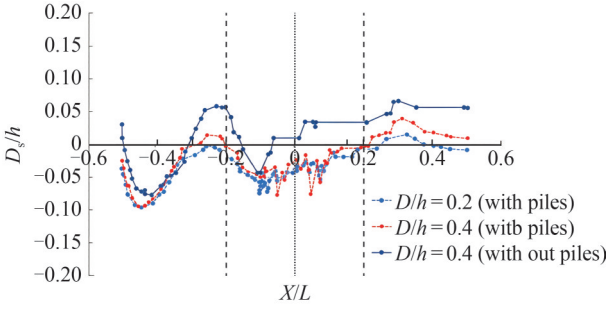
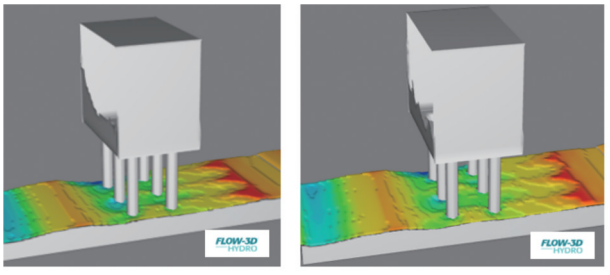
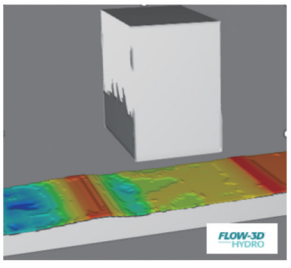


Figure 17 Longitudinal seabed outline at the middle of the contour map around the breakwater models for $Kh = 1$



(a) $D/h = 0.2$ (closely spaced piles)

(b) $D/h = 0.4$ (closely spaced piles)



(c) $D/h = 0.4$ (large spaced piles)

Figure 18 Distribution of scour and deposition zones around the three breakwater models for $Kh = 1$

4.2.4 Seabed changes for Kh=0.46

Figure 19 presents the numerical sea bed morphology of the three breakwater models when Kh = 0.46 for three cases of changing the relative breakwater drafting D/h. The first model for D/h = 0.2 (closely spaced piles), the second model for D/h = 0.4 (closely spaced piles), and the third model for D/h = 0.4 (large spaced piles). The first model showed a big scour hole formed seaward with various deposition heights distributed along the contour map. The extreme relative seaward scour depth D_{smax}/h is 0.05. The extreme relative scour deepness around the piles D_{smax}/h is 0.12, and the maximum relative shoreward deposition height D_{dmax}/h is 0.05. Different small deposition zones formed round the piles with D_{dmax}/h 0.025. Extreme relative scour hole length L_{smax}/l seaward and round the piles are 0.02 and 0.06. The second model is given that big scour zones formed around the second shoreward raw of piles with D_{smax}/h is 0.05. Also, the big deposition height viewed at the nose of the piles D_{dmax}/h is 0.06. A very small scour zone formed seaward with D_{smax}/h is 0.02. L_{smax}/l seaward and around the piles are 0 and 0.03. The consequence of the third model on the seabed changes is actual minor as it can be ignored. Successive areas of scour and deposition are formed along the contour map. The extreme relative scour depth under the breakwater system D_{smax}/h is 0.025. The extreme relative seaward scour deepness D_{smax}/h is 0.005. The maximum relative deposition height shoreward D_{dmax}/h is 0.03. The scour hole length L_{smax}/l seaward is 0.08. The numerical longitudinal sea bed shape at the center of the contour plan for the three breakwater models for different values of changing the relative breakwater drafting D/h is offered in Figure 20. The figure displays that the sea bed morphology is not uniform but varies from scour zones to deposition zones due to the high confusion caused by the interaction among the partial standing waves and the reflected waves from the breakwater body beside the breaking waves causing horseshoe vortex in front of the breakwaters. The distribution of the scour and deposition zones exerted from FLOW-3D HYDRO when Kh = 0.46 for the three breakwater models is presented in Figure 21.

Figure 22 presents the relation between the dimensionless wave number Kh and the seaward maximum relative scour depth D_{smax}/h. The figure illustrated that the equilibrium scours are induced when Kh increases to 0.80 and then starts to decrease. That refers to the rise in the orbital velocity and the maximum bottom pressure. The extreme relative scour depth ranged between 0.10 and 0.12 when the dimensionless wave number Kh oscillated from 0.70 to 0.90 seaward represents 12% relative to the water depth.

Figure 23 presents the relation between the dimensionless wave number Kh and the extreme relative seaward hole length L_{smax}/l for three models. The three models indicated that the maximum relative seaward hole length increased by increasing the dimensionless wave number

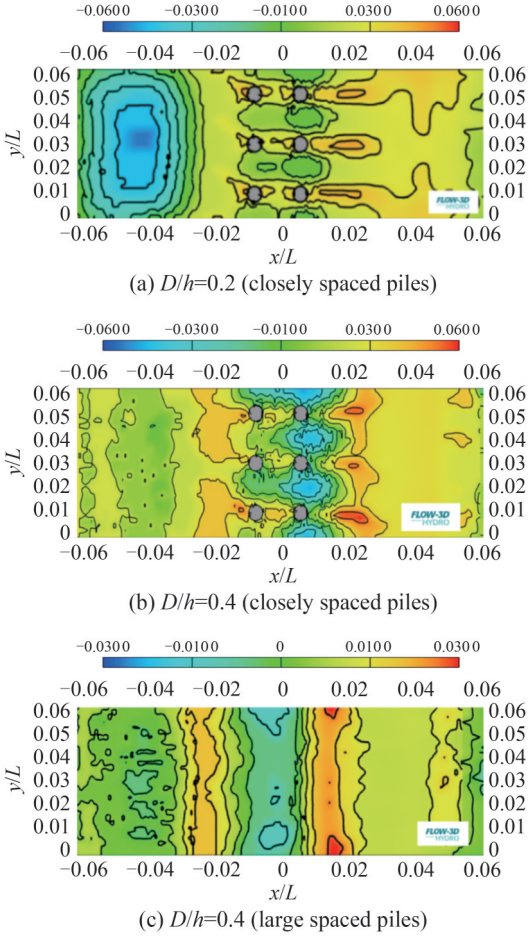


Figure 19 Contour maps of the seabed changes around the different caisson breakwater models when Kh = 0.46

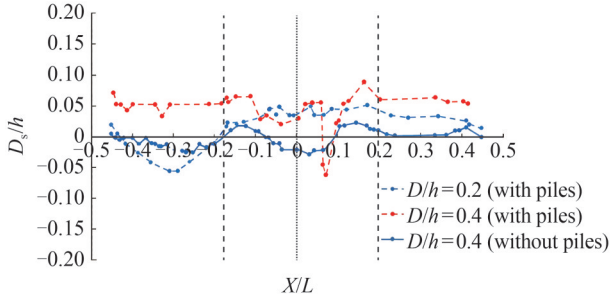
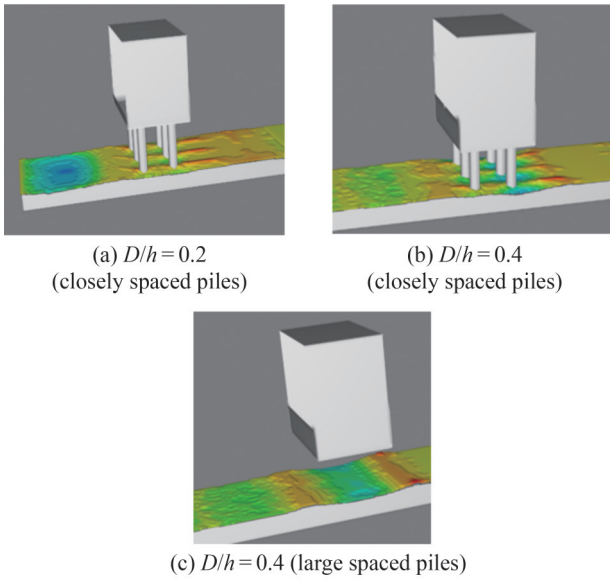


Figure 20 Longitudinal seabed outline at the mid of the contour map around the breakwater models for Kh = 0.46

Kh. For the first and the second model, it increased when the Kh reached 1.00 while for the third model, it increased when the Kh reached 0.85. Then it began to decrease for the three models.

Figure 24 presents the relation between the dimensionless wave number Kh and the extreme relative shoreward deposition height D_{dmax}/h for the three models. For the first model, the maximum relative deposition height increased when Kh reached 0.80. Then it decreased until reached



(a) $D/h = 0.2$ (closely spaced piles)

(b) $D/h = 0.4$ (closely spaced piles)

(c) $D/h = 0.4$ (large spaced piles)

Figure 21 Distribution of scour and deposition zones around the three breakwater models for $Kh = 0.46$

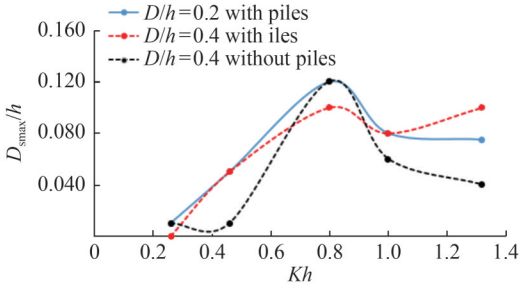


Figure 22 The consequence of the dimensionless wave number Kh on the seaward maximum relative scour depth D_{smax}/h

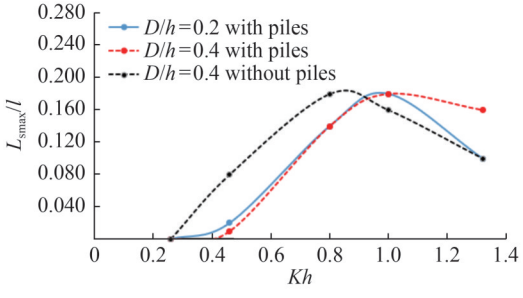


Figure 23 The consequence of the dimensionless wave number Kh on the seaward extreme relative length L_{smax}/l

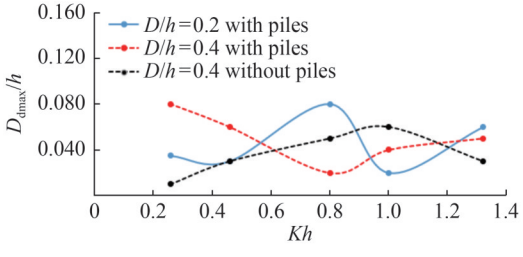


Figure 24 The consequence of the dimensionless wave number Kh on the shoreward maximum relative deposition height D_{dmax}/h

$Kh = 1.00$ and started to increase slowly again. For the second model, it decreased when Kh reached 0.80 and then started to increase slowly again. For the third model, it increased when Kh reached 1.00 and then started to decrease again. The maximum deposition height D_{dmax} shoreward was found to be 9% relative to the water depth.

Figure 25 presents the relation between dimensionless wave number Kh and the maximum relative scour depth around the piles D_{smax}/h for the two models. For the first model, the maximum relative scour deepness increased when Kh reached 0.50 and then started to decrease until Kh reached 0.85 and then started to increase again. For the second model, the maximum relative scour depth decreased when Kh reached 0.60 and then started to increase again. The extreme scour deepness around the piles D_{smax} was initiated to be 8% relative to the water depth.

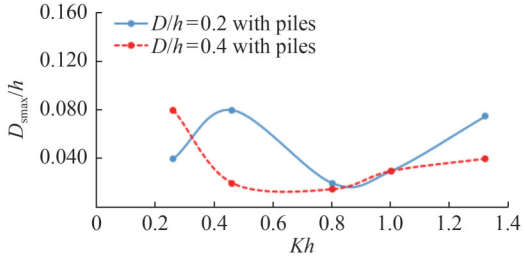


Figure 25 The consequence of the dimensionless wave number Kh on the shoreward maximum relative deposition height D_{smax}/h

Figure 26 presents the relation between dimensionless wave number Kh and the maximum relative hole length around the piles L_{smax}/l for two models. For the first model, L_{smax}/l increased until Kh reached 0.45 then decreased until Kh reached 0.80 and started to increase again quickly to $Kh = 1.00$ and gradually slowly increased to $Kh = 1.32$. For the second model, L_{smax}/l decreased until Kh reached 0.45 and then started to increase again.

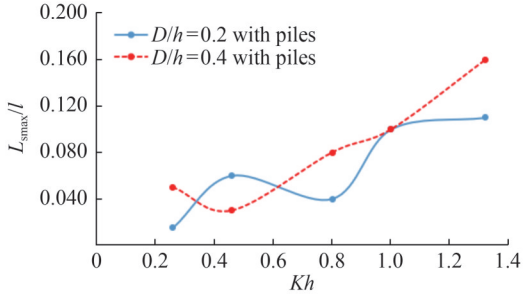


Figure 26 The effect of the dimensionless wave number Kh on the maximum relative scour depth around the piles L_{smax}/l

4.3 Influence of changing the breakwater section on the scour process

The primary objective of this analysis is to determine

the optimal cross-section of the caisson breakwater and assess its impact on the progression of scour. To achieve this, two scenarios were considered. In the first scenario, the caisson base is increased by 0.25 W and 0.50 W on both sides. The second scenario the breakwater width is increased by 0.25 W and 0.50 W on both sides.

4.3.1 Increasing the breakwater base (Both Sides)

The second configuration examines widening the breakwater base symmetrically on both sides by 0.25 W and 0.50 W, as illustrated in Figure 27.

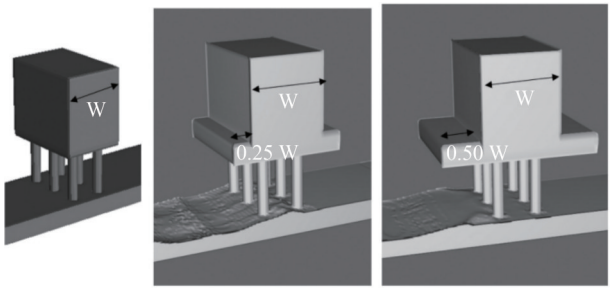


Figure 27 The second scenario of increasing the breakwater base from two sides with two values

Figure 28 presents the influence of these base extensions on scour development and highlights the differences in scour and deposition patterns between the original design and the two modified geometries.

As shown in Figure 28(b), enlarging the caisson base shifts the scour zone further seaward. A pronounced scour region develops offshore, with a maximum normalized scour depth of $D_{smax}/h = 0.130$, representing an increase of 128.07% relative to the baseline model. A notable deposition zone also forms between the two pile rows, reaching $D_{dmax}/h = 0.100$.

Figure 28(c) demonstrates that extending the breakwater base by 0.50W on both sides produces a substantial deposition zone seaward beneath the expanded base ($D_{dmax}/h = 0.080$) and a significant offshore scour area ($D_{smax}/h = 0.080$), corresponding to a 40.35% increase compared to the original configuration. This indicates that widening the caisson base by 0.50 W on each side is more effective in mitigating scour progression around the piles. The modification successfully redirects the scour away from the caisson structure, though it results in a 40.35% increase in scour depth offshore.

The seabed deformation along the centerline of the domain for the three configurations is presented in Figure 29.

4.3.2 Increasing the breakwater width (two sides)

The two scenarios of increasing the breakwater cross section with two values is shown in Figure 30.

Figure 31 illustrates the effect of increasing the breakwater width from both sides by 0.25 W and 0.50 W, respec-

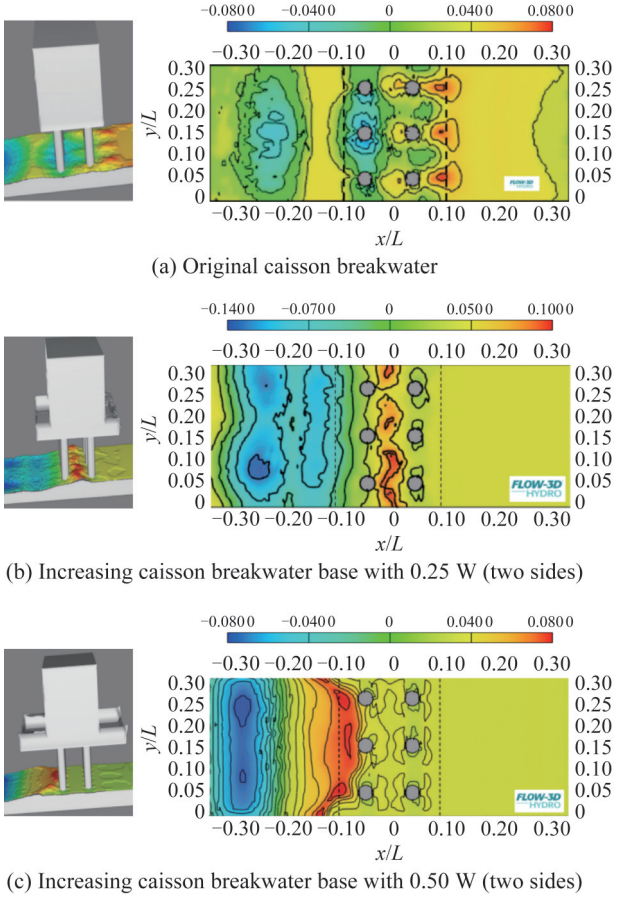


Figure 28 The effect of increasing the breakwater base (two sides) on the scour process for $Kh = 1.32$, and $D/h = 0.20$

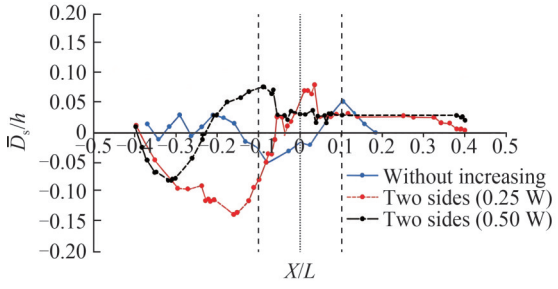


Figure 29 Longitudinal seabed profile at the middle of the contour map around the three caisson models in case of increasing the breakwater base on two sides for $Kh = 1.32$

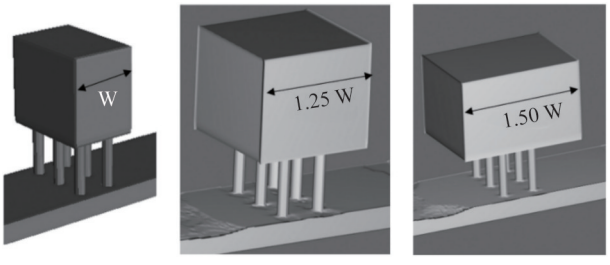
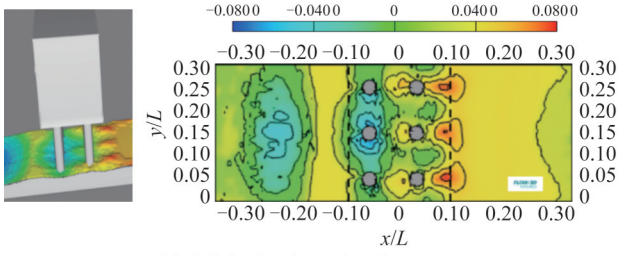
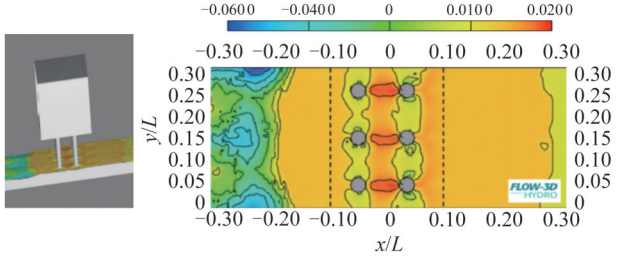


Figure 30 The third scenario of increasing the breakwater cross-section with two values

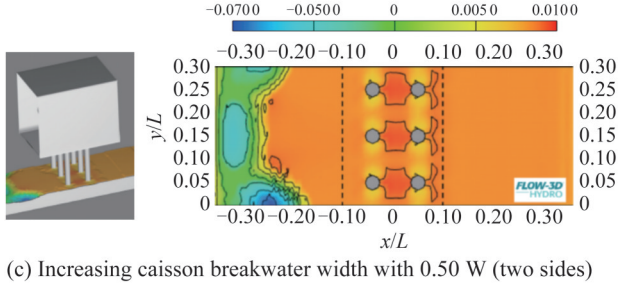
tively, on scour development. It also shows the differences in scour and deposition distributions between the original model and the two optimized sections. Figure 31(b) shows that increasing the caisson width by 0.25 W on both sides results in the scour zone moving farther away from the piles and concentrating seaward, with (D_{smax}/h = 0.057), which represents no increase in scour depth, As the scour depth remains constant. Deposition areas form shoreward and around the piles, with a deposition zone appearing between the two rows of piles, having (D_{dmax}/h = 0.018). Figure 31(c) shows that increasing the caisson width by 0.50 W causes the scour zone to shift even farther seaward, with (D_{smax}/h = 0.070), an increase of 22.81% compared to the original case. All areas around the piles and shoreward are deposition zones, with the maximum deposition height appearing between the piles at (D_{dmax}/h = 0.070). Therefore, increasing the breakwater width by 0.25 W is more effective in controlling scour progression than increasing it by 0.50 W. This approach successfully redirects the scour away from the breakwater while keeping the scour depth constant. The deformation of the seabed profile along the contour map for the three models at the center of the domain is shown in Figure 32.



(a) Original caisson breakwater



(b) Increasing caisson breakwater width with 0.25 W (two sides)



(c) Increasing caisson breakwater width with 0.50 W (two sides)

Figure 31 The effect of increasing the breakwater width (two sides) on the scour process for Kh = 1.32, and D/h = 0.20

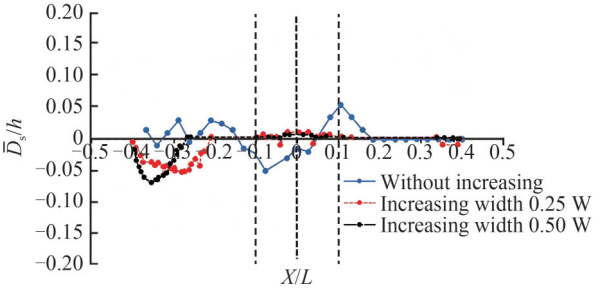


Figure 32 Longitudinal seabed profile at the middle of the contour map around the three caisson models in case of increasing the breakwater width for Kh = 1.32

5 Conclusions

The study employed the FLOW-3D HYDRO model to investigate the morphological impacts of a semi-immersed caisson breakwater supported by a group of piles, subjected to regular waves. The primary focus was to assess the changes in the seabed beneath and around the breakwater structure. Several factors were considered, including wave height, wavelength, wave period, the draft of the breakwater, and the spacing between the piles, all under a constant water depth. The study led to significant conclusions regarding the influence of these parameters on seabed alterations. Two scenarios were considered, including the effect of altering the caisson's cross-section on controlling scour progression.

(1) The results revealed a strong agreement between the numerical simulations and experimental data for scenarios involving widely spaced piles, as indicated by a low mean square error. In contrast, cases with intermediate wave conditions exhibited lower convergence between the numerical and experimental outcomes, particularly in the presence of piles, which was associated with a higher mean square error.

(2) The maximum relative seaward erosion depth (D_{smax}/h) ranged between 0.10 and 0.12 when the dimensionless wave number (Kh) was between 0.7 and 0.9. Equilibrium scours were observed when Kh reached 0.80. Additionally, the extreme virtual scour hole length (L_{smax}/l) varied between 0.16 and 0.18 when the dimensionless wave number (Kh) ranged from 0.9 to 1.0.

(3) At a dimensionless wave number of Kh = 0.80, the highest recorded maximum relative shoreward deposition height (D_{dmax}/h) was 0.08, observed with a relative breakwater draft of D/d = 0.2 for pile-supported structures. Conversely, a lower value of 0.015 was recorded when the relative breakwater draft (D/d) increased to 0.4, also in the presence of piles.

(4) The maximum virtual scour depth around the piles (D_{smax}/h) peaked when the relative breakwater draft (D/d) was 0.2 for pile-supported structures. However, as the rela-

tive breakwater draft increased to 0.4, a lower value was observed, occurring when the dimensionless wave number Kh was 0.46.

(5) The extreme relative scour depth around the piles (D_{smax}/h) was highest for structures with piles and a relative breakwater draft (D/d) of 0.2, while it was lowest when the draft increased to 0.4 at $Kh = 0.46$.

(6) In the case of increasing the breakwater width by 0.25 W, it was found to successfully divert the scour away from the breakwater while maintaining a constant scour depth. In contrast, increasing the width by 0.50 W resulted in both the diversion of the scour and an increase in its depth. Therefore, increasing the breakwater width by 0.25 W is considered one of the best outcomes and an ideal solution for controlling scour.

(7) Increasing the caisson base by 0.50 W on both sides proved more effective in controlling the progression of scour around the piles. This approach successfully diverted the scour away from the caisson breakwater, resulting in a 40.35% increase in scour depth with restricting the scour's location.

Funding Supported by the Slovak Research and Development Agency under the Contract no. APVV-20-0281.

Competing interests The authors have no competing interests to declare that are relevant to the content of this article.

References

Ahmad N, Bihs H, Myrhaug D, Kamath A, Arntsen A (2019) Numerical modeling of breaking wave-induced seawall scour. Coastal Engineering 150: 108-120. https://doi.org/10.1016/j.coastaleng.2019.03.010

Baykal C, Sumer BM, Fuhrman DR, Jacobsen NG, Fredsoe J (2015) Numerical investigation of flow and scour around a vertical circular cylinder. Philosophical Transactions of the Royal Society A: Mathematical, Physical and Engineering Sciences 373: 20140104. https://doi.org/10.1098/rsta.2014.0104

Baykal C, Sumer BM, Fuhrman DR, Jacobsen NG, Fredsoe J (2017) Numerical simulation of scour and backfilling processes around a circular pile in waves. Coastal Engineering 122: 87-107. https://doi.org/10.1016/j.coastaleng.2017.01.004

Dean RG (1987) Coastal armoring: Effects, principles and mitigation. Proceedings of the Coastal Engineering Conference 3: 1843-1857. https://doi.org/10.1061/9780872626003.135

Gíslason K, Fredsoe J, Deigaard R, Sumer BM (2009) Flow understanding waves. Part 1. Shear stress distribution, energy flux, and steady streaming. Coastal Engineering 56: 341-362. https://doi.org/10.1016/j.coastaleng.2008.11.001

Heikal EM, Koraim AS, Elsebaie ME, Elbagory IA (2022) Seabed changes and hydrodynamic characteristics of the caisson breakwater supported on piles. NeuroQuantology 20: 10711-10726. https://doi.org/10.14704/nq.2022.20.10.NQ551037

Kamphuis JW, Rakha KA, Jui J (1992) Hydraulic model experiments on seawalls. Coastal Engineering 1992: 1272-1284

Koraim A (2005) Effect of pile system characteristics on the caisson breakwater efficiency and seabed changes. Mansoura Engineering Journal 31: 53-68. https://doi.org/10.21608/bfemu.2020.129185

Kraus NC, McDougal WG (1996) The effects of seawalls on the beach: Part I, an updated literature review. Journal of Coastal Research 12(3): 691-701

Lin IF, Tseng IF, Lee CP (2014) A three-dimensional numerical model for evaluation of seabed scour potential around a breakwater in Mailiao. Oceans 2014-Taipei: 1-5. https://doi.org/10.1109/OCEANS-TAIPEI.2014.6964551

McDougal WG, Kraus NC, Ajiwibowo H (1997) The effects of seawalls on the beach: Part II, numerical modeling of super tank seawall tests. Oceanographic Literature Review 3(44): 283

Myrhaug D, Ong MC (2009) Random wave-induced scour at the trunk section of a breakwater. Coastal Engineering 56: 688-692

Roelvink JA, Stive MJF (1989) Bar-generating cross-shore flow mechanisms on a beach. Journal of Geophysical Research: Oceans 94: 4785-4800

Sumer BM, Fredsoe J (2000) Experimental study of 2D scour and its protection at a rubble-mound breakwater. Coastal Engineering 40: 59-87. https://doi.org/10.1016/S0378-3839(00)00006-5

Sutherland J, Obhrai C, Whitehouse RJS, Pearce A (2006) Laboratory tests of scour at a seawall. Proceedings 3rd International Conference on Scour and Erosion, CURNET, Gouda, The Netherlands

Tsai CP, Chen HB, You SS (2009) Toe scour of seawall on a steep seabed by breaking waves. Journal of Waterway, Port, Coastal, and Ocean Engineering 135: 61-68. https://doi.org/10.1061/(ASCE)0733-950X(2009)135:2(61)

Vitousek S, Barnard PL, Fletcher CH, Frazer N, Erikson L, Storlazzi CD (2017) Doubling of coastal flooding frequency within decades due to sea-level rise. Scientific Reports 7: 1-9

Wang C, Liang F, Yu X (2017) Experimental and numerical investigations on the performance of sacrificial piles in reducing local scour around pile groups. Natural Hazards 85: 1417-1435. https://doi.org/10.1007/s11069-016-2634-0

Wei G, Brethour J, Grünzner M, Burnham J (2014) The sedimentation scours model in FLOW-3D. Flow Science Rep, 1-26. http://www.flow3d.co.kr/wp-content/uploads/FloSci-TN99_The-Sedimentation-Scour-Model.pdf

Xie Z (1981) Scouring patterns in front of vertical breakwaters and their influences on the stability of the foundations of the breakwaters. Department of Civil Engineering. Delft University of Technology, Delft, The Netherlands, 66

Yang M, Tang Y, Zhao F, Xu S, Fang G (2024) Numerical simulation of local scour around a square artificial reef. Journal of Offshore Mechanics and Arctic Engineering 146: 021202. https://doi.org/10.1115/1.4062591